

Room-Temperature Quantum Bit Storage Exceeding 39 Minutes Using Ionized Donors in Silicon-28

Kamyar Saeedi,¹ Stephanie Simmons,² Jeff Z. Salvail,¹ Phillip Dluhy,¹ Helge Riemann,³ Nikolai V. Abrosimov,³ Peter Becker,⁴ Hans-Joachim Pohl,⁵ John J. L. Morton,⁶ Mike L. W. Thewalt^{1*}

Quantum memories capable of storing and retrieving coherent information for extended times at room temperature would enable a host of new technologies. Electron and nuclear spin qubits using shallow neutral donors in semiconductors have been studied extensively but are limited to low temperatures (≤ 10 kelvin); however, the nuclear spins of ionized donors have the potential for high-temperature operation. We used optical methods and dynamical decoupling to realize this potential for an ensemble of phosphorous-31 donors in isotopically purified silicon-28 and observed a room-temperature coherence time of over 39 minutes. We further showed that a coherent spin superposition can be cycled from 4.2 kelvin to room temperature and back, and we report a cryogenic coherence time of 3 hours in the same system.

A long-term, portable quantum storage register operating at room temperature would be an important advance in realizing the potential of quantum computation (1, 2) and new technologies such as quantum money (3, 4). Solid-state quantum systems have reached a coherent

storage time (T_2) of ~ 2 s for the nuclear spin of a ^{13}C atom coupled to a nitrogen-vacancy (NV) center in diamond at room temperature (5). Another promising semiconductor qubit system uses the electron and/or nuclear spins of neutral shallow donor impurities (D^0) such as ^{31}P in Si (6–8). The

nuclear spin of neutral ^{31}P in isotopically purified ^{28}Si can reach a coherence time of 180 s (9); however, like all shallow D^0 , this is an inherently low-temperature system. Even at 4.2 K, the nuclear spin T_2 is limited by the electron spin relaxation time, T_1 (9), which decreases very rapidly with increasing temperature, dropping to a few milliseconds at 10 K (10); in addition, the donors begin to thermally ionize above ~ 30 K.

Here we show that the nuclear spin of the ionized donor (D^+) has important advantages over that of D^0 and is not limited to operation at cryogenic temperatures. In two recent studies on the D^+ nuclear spin in natural Si at cryogenic temperatures, one on an ensemble (11) and one on a single ^{31}P atom (12), the nuclear spin T_2 for D^+ was found to be considerably longer than that for D^0 , because the removal of the electron spin eliminated decoherence associated with the electric field noise arising from the nearby electrolytes and Si/SiO₂ interface. The resulting D^+ T_2

¹Department of Physics, Simon Fraser University, Burnaby, BC, V5A 1S6, Canada. ²Department of Materials, Oxford University, Oxford OX1 3PH, UK. ³Leibniz-Institut für Kristallzüchtung, 12489 Berlin, Germany. ⁴PTB Braunschweig, 38116 Braunschweig, Germany. ⁵VITCON Projectconsult, 07743 Jena, Germany. ⁶London Centre for Nanotechnology, University College London, London WC1H 0AH, UK.

*Corresponding author. E-mail: thewalt@sfu.ca

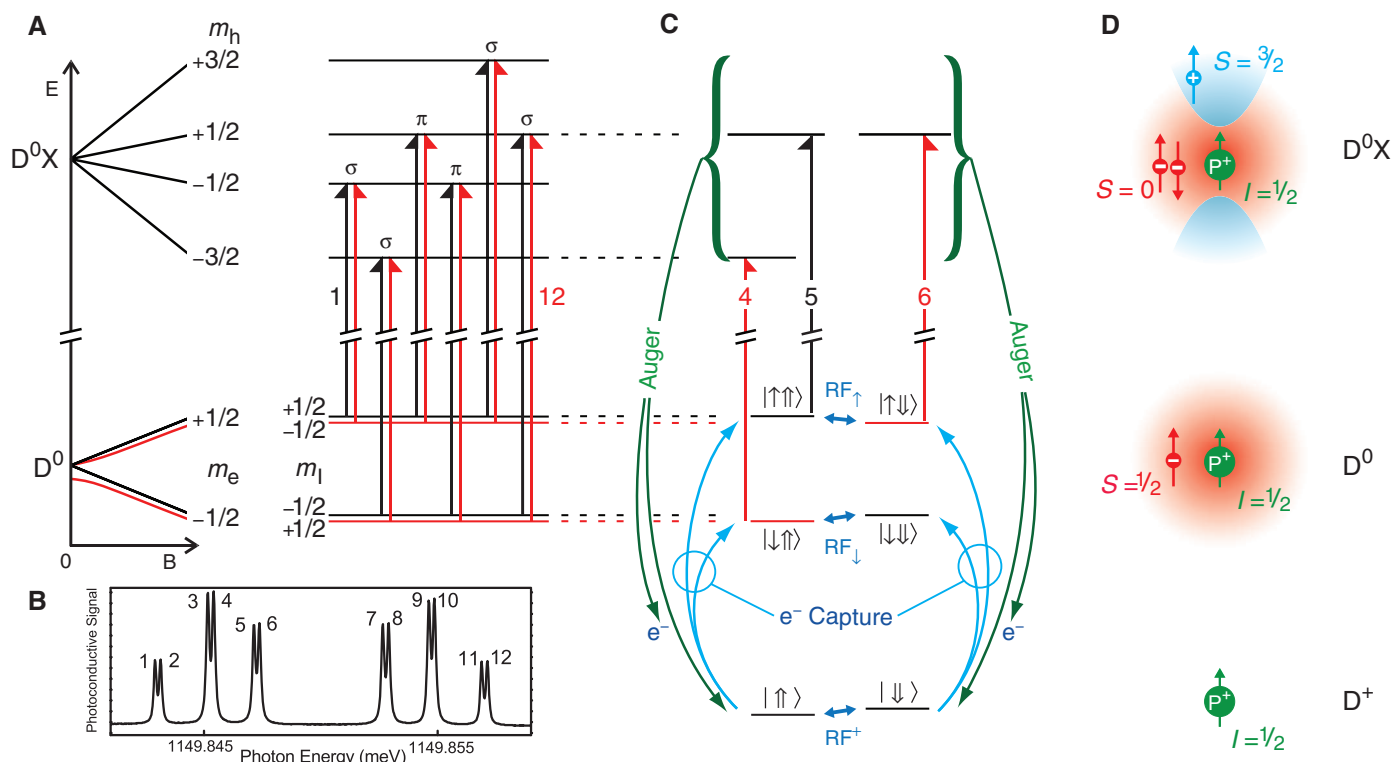


Fig. 1. Energy levels and transitions of the P neutral donor (D^0), donor bound exciton (D^0X), and ionized donor (D^+). (A) The Zeeman splittings of the D^0 and D^0X states are shown from $B_0 = 0$ to $B_0 = 845.3$ G, along with the dipole-allowed optical transitions. (B) Photoconductive readout spectrum without any D^0 hyperpolarization. (C) The specific optical transitions (lines 4, 5, and 6) and nuclear magnetic resonance transitions (RF_+ , RF_- , and RF^+) used here to hyper-

polarize, manipulate, and read out the nuclear spins. The magnitude of the D^+ Zeeman splitting (RF^+) has been exaggerated to show the ordering of the D^+ states, and the small nuclear Zeeman energy is ignored for the D^0X states. Although the energy differences between the D^0 and D^0X levels are precisely fixed in ^{28}Si , the D^+ energy is not well defined because of the kinetic energy of the e^- . (D) Sketches of the spins and charge densities of D^+ , D^0 , and D^0X .

of tens of milliseconds was well accounted for (11, 12) by spectral diffusion from the ~5% of ^{29}Si occurring in the natural Si samples (13). We removed this source of spectral diffusion by using highly enriched ^{28}Si and dynamic decoupling.

The sample used here and in the previous study of D^0 (9) was enriched to 99.995% ^{28}Si and contained $\sim 5 \times 10^{11} \text{ cm}^{-3}$ of ^{31}P and $5 \times 10^{13} \text{ cm}^{-3}$ of the acceptor B, making it p-type (14). In equilibrium at low temperature one would expect all donors to be D^+ , with an equal number of ionized acceptors, but this equilibrium is reached very slowly at these low concentrations (15). Weak above-gap excitation provided by a 1047-nm laser photoneutralizes almost all of the donors and acceptors. Highly enriched ^{28}Si provides a “semiconductor vacuum” host for dopants, allowing for the optical hyperpolarization and readout of D^0 nuclear spin states (9, 16). We additionally used optical transitions to fully ionize the spin-polarized D^0 at low temperature, after which T_1 or T_2 measurements can be carried out on D^+ at either cryogenic or room temperature. After this, with the sample at cryogenic temperature, the D^+ atoms are optically reneutralized, and the remaining D^0 polarization is read out optically. Once ionized, virtually all donors will remain ionized indefinitely, independent of temperature, provided that above-gap light is excluded. Above ~30 K, the excess acceptors ionize, providing a background of free holes, and nearer room temperature, thermally generated free electrons will also be present (14). These free carriers could affect the D^+ nu-

clear spin polarization and coherence times, but our results show that long-term coherent storage at room temperature is still possible.

The optical transitions between D^0 and the donor bound exciton (D^0X) used for hyperpolarization, readout, and donor ionization are shown in Fig. 1. In Fig. 1C, the four D^0 hyperfine levels are labeled by their electron spin (\uparrow or \downarrow) and nuclear spin (\uparrow or \downarrow) (the $|\uparrow\uparrow\rangle$ and $|\downarrow\downarrow\rangle$ labels are approximate at low B_0 because of hyperfine mixing). The D^0X atoms decay with near-unity efficiency through the Auger process (17) to give D^+ and free electrons (e^-), which are eventually recaptured to return D^+ to D^0 . The Auger decay process is central to both the D^0 hyperpolarization and hyperfine state readout using resonant D^0X photoconductivity, as illustrated in the sequence used to measure the coherence time of D^+ nuclear spins [Fig. 2A and (14)]. It consists of optical and radio-frequency (RF) pulses to hyperpolarize the nuclear spins (steps {1 to 3}), fully ionize the donors {4}, coherently manipulate the D^+ nuclear spin {6 to 8}, reneutralize the donors {10}, and read out the resulting spin populations {11 to 14}. By step {5}, we estimate that over 90% of the ^{31}P atoms are both ionized and polarized into $|\uparrow\rangle$. Single-shot readouts of D^+ , polarized into either $|\uparrow\rangle$ or $|\downarrow\rangle$ and then reneutralized, are shown in Fig. 2, B to D, contrasting our previous (9) readout method optimized for D^0 (Fig. 2B) with the improved readout used here (Fig. 2, C and D). Details of the preparation and readout schemes are found in (14). Analysis of the data

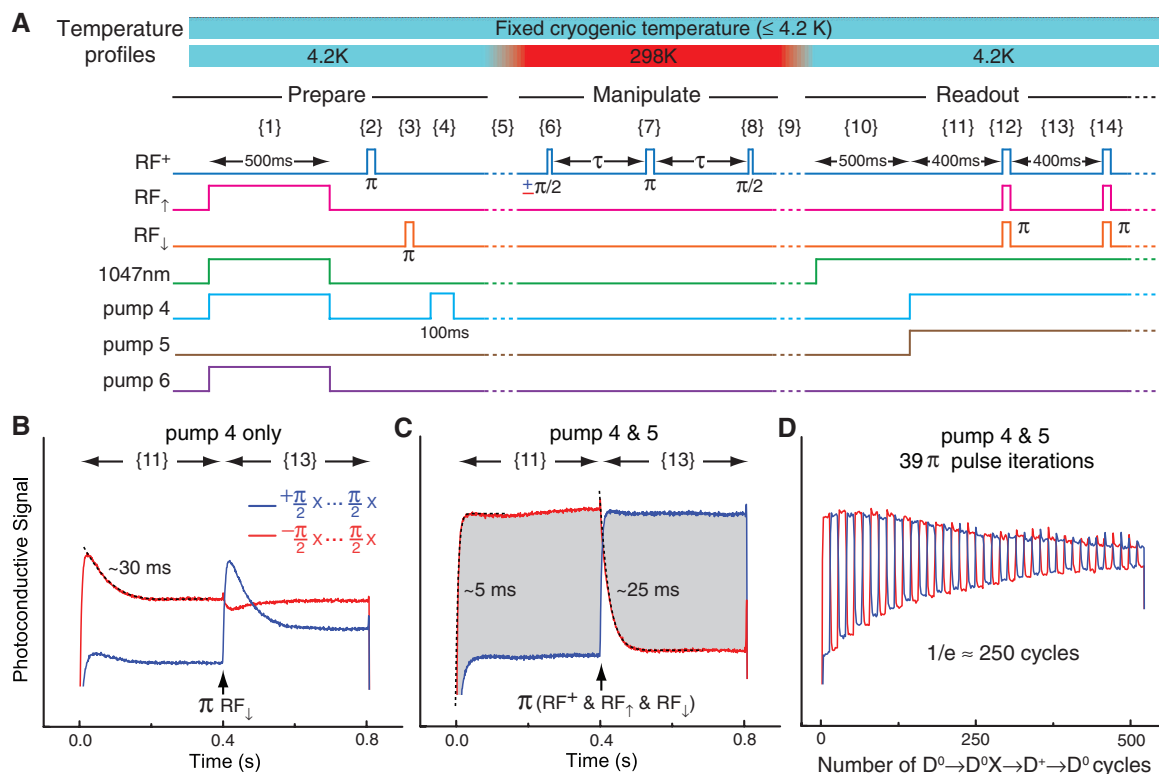
in Fig. 2, C and D, shows that the $\text{D}^0 \rightarrow \text{D}^0\text{X} \rightarrow \text{D}^+ \rightarrow \text{D}^0$ readout cycle can be repeated at least 250 times before the nuclear polarization decays by $1/e$ (14), which is an underestimate given that much of the decay in Fig. 2D is due to imperfections in the readout π pulses. A similar insensitivity of the nuclear spin polarization to repeated donor charge cycles has been reported for readout of a single ^{31}P nuclear spin (12) and for ensemble measurements using electrically detected magnetic resonance (18).

We used two different temperature profiles to measure T_1 and T_2 , as shown above Fig. 2A; either a fixed temperature at or below 4.2 K, or T_1 or T_2 measurements at room temperature (298 K), with the polarization and readout steps at 4.2 K. The measurement RF pulse sequence is shown for a simple Hahn echo ($\pi/2 - \pi - \pi/2$). The temperature is changed only while the D^+ nuclear spin is in an eigenstate in the Z basis (i.e., in the $|\downarrow\rangle$ or $|\uparrow\rangle$ state). This ensures that the nuclear spin is sensitive only to T_1 relaxation processes while the temperature is changing. Later we explored a third profile, changing the temperature while the nuclear spin was in a superposition state.

In Fig. 3A we show the D^+ nuclear spin T_1 measured at 1.9 K and room temperature [the Hahn echo sequence is replaced with either no operations, leaving the nuclear spin polarization unchanged, or a π pulse, which inverts it (14)]. The D^+ T_1 at cryogenic temperature was so long that no decay could be observed over 2 hours, and at room temperature T_1 was over an hour.

Fig. 2. Initialization, manipulation, and readout protocols.

(A) The laser and RF sequences used to prepare D^+ in the $|\uparrow\rangle$ state (steps {1} to {4}), manipulation of D^+ spins for the case of a Hahn echo ({6} to {8}), and readout of the resulting Z component ({10} to {14}...). At the top are the two temperature profiles relevant to Fig. 3: either a constant temperature ≤ 4.2 K or 4.2 K during preparation and readout, with a ramp up to 298 K taking ~6 min {5}, a constant 298 K during the D^+ manipulation period, and a ramp down to 4.2 K taking ~4 min {9}. Each measurement was performed twice, with opposite signs of the initial $\pi/2$ pulse {6}. (B) Single-shot readout of D^+ polarized $|\uparrow\rangle$ (red) or $|\downarrow\rangle$ (blue) using our previous method optimized for D^0 readout is compared with (C), the improved scheme for D^+ readout (14). The detected signal is proportional to the shaded area. (D) The cycle shown in (C) extended to 39 π pulse inversions (16 s).



Even a short thermal cycle up to room temperature and back resulted in a ~30% loss in nuclear spin polarization as compared to the same measurement at a constant 4.2 K, so all room-temperature decay data are normalized to unity for the shortest time (2 min at 298 K). Figure 3B shows single-shot Hahn echo decay data at 4.2 K revealing increasing phase noise with increasing delay time, probably arising from low-frequency magnetic field fluctuations. This phase noise was eliminated from the 1.9 K data by using maximum magnitude detection (14). The Hahn echo T_2 of about 30 s measured at or below 4.2 K is well explained by spectral diffusion due to the residual (46 parts per million) ^{29}Si nuclear spins

present in the sample (13). Also shown is single-shot Hahn echo data at room temperature, where the long cycle time made the use of maximum magnitude detection impractical, so that the phase noise could not be eliminated, and the apparent Hahn echo T_2 was reduced to ~8 s.

We have demonstrated (9) that dynamic decoupling using the XY-16 sequence of π pulses (19) is effective for reducing the effect of low-frequency noise on donor nuclear spins while maintaining arbitrary initial states. In Fig. 3C we show the results of using this sequence to replace the single π pulse of the Hahn echo (for all XY-16 results shown here, the time 2τ between π pulses was 8 ms). At 1.2 K the coherence decay follows

a single exponential, with a T_2 of 180 min, whereas at 1.9 K and 4.2 K there is an early component of a faster decay (time constant ~12 min), followed by a decay consistent with a T_2 of 180 min. We believe that this initial faster decay is due to charge dynamics in the sample after illumination, probably from D^- and A^+ centers, which are frozen out at the lowest temperature (20). It may be related to the ~30% loss in nuclear polarization observed in even short cycles from cryogenic to room temperature and back. In Fig. 3D we show a room-temperature T_2 decay of 39 min. This is a lower bound, because the same XY-16 sequence applied to a $\pm Z$ state yields a decay constant of 50 min, which is substantially shorter than the

Fig. 3. Measured T_1 and T_2 times for the $^{31}\text{P}^+$ nuclear spin at cryogenic and room temperature. (A) The decay of the nuclear spin polarization (along Z), parameterized by T_1 , is shown for 1.9 and 298 K. (B) Single-shot Hahn echo T_2 measurements are shown at 298 and 4.2 K, the latter (green dots) showing increasing phase noise with increasing delay. The effect of phase noise can be suppressed by using maximum magnitude detection (14), as shown for data taken at 1.9 K. (C) T_2 decays using the XY-16 decoupling sequence at cryogenic temperatures. The 1.9 and 4.2 K data were fit using biexponentials, with the longer component set to 180 min. (D) The T_2 decay at 298 K using XY-16 decoupling, together with the observed decay of a $\pm Z$ state using XY-16 decoupling under identical conditions.

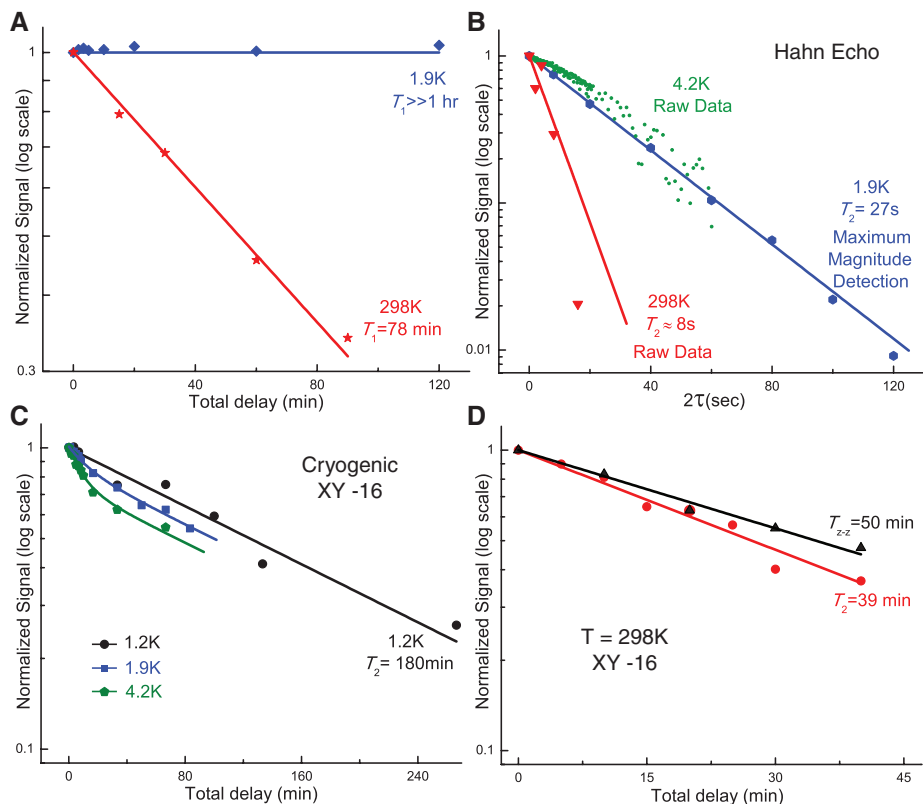
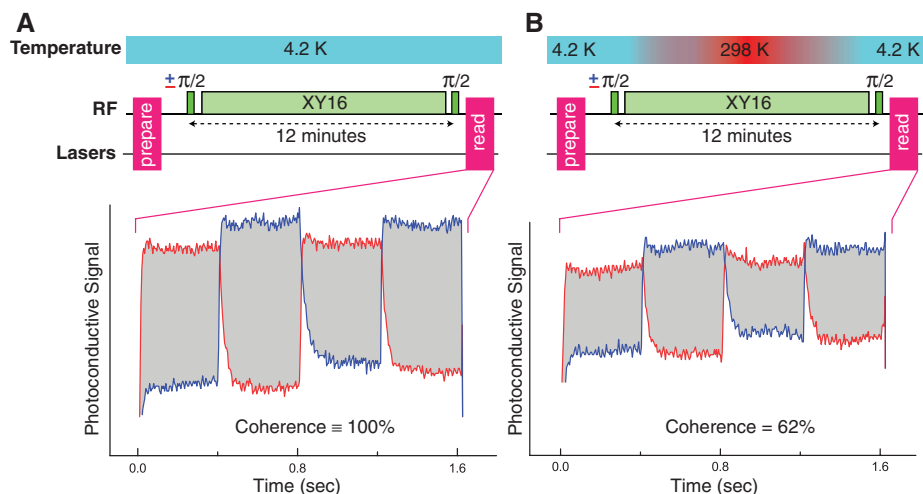


Fig. 4. Cycling D^+ , while in a nuclear spin superposition state, from 4.2 K to room temperature and back. (A) A measurement at a constant temperature of 4.2 K, with XY-16 decoupling over a 12-min period, is compared to (B), where the nuclear spins are placed into a coherent superposition at 4.2 K and the XY-16 decoupling sequence is begun, followed by a ~6-min ramp to 298 K, 2 min at 298 K, and a ~4-min ramp back down to 4.2 K, after which the remaining coherence is read out. The preparation and readout sequences are as in Fig. 2A. A comparison of (A) and (B) shows that 62% of the spin coherence remains after the temperature cycle, which is equivalent to a state fidelity of 81%.



78-min T_1 , indicating that pulse errors in the XY-16 sequence contribute significantly to the observed decay and are also likely to contribute to the 180-min T_2 observed at cryogenic temperatures.

The low-temperature nuclear spin T_2 of ≥ 180 min demonstrates that the XY-16 sequence is very effective in suppressing decoherence arising from slow spectral diffusion caused by the remaining ^{29}Si . Whereas the cryogenic Hahn echo T_2 reported here for D^+ is slightly shorter than that reported earlier (10) for D^0 , XY-16 dynamic decoupling extends the observed coherence time by a factor of 400 for D^+ but only by ~ 4.4 for D^0 . This suggests a very different decoherence process for the D^0 case (14).

These long coherence times for the D^+ nuclear spin should be achievable even when the donor is placed near an interface in a nanodevice, as long as the temperature is low enough that flips or flip-flops of electron spins at the interface are suppressed. The shorter 39-min T_2 measured at room temperature could arise from carrier-induced magnetic field fluctuations, whose effect is not completely suppressed by the dynamical decoupling, combined with a higher error in the RF pulses (15). The observed room-temperature T_2 is also compatible with the accumulated phase error from the small probability of the donor being in the D^0 ground state at room temperature. The observed room-temperature T_2 considerably exceeds that reported (21) for ^{29}Si in natural Si using homonuclear decoupling. Given that ^{29}Si should not be more sensitive to free carriers than D^+ , this probably results from difficulty in completely decoupling the ^{29}Si at the high concentration present in natural Si.

Finally, we demonstrated the ability to change the sample temperature while the D^+ nuclear spin was in a coherent superposition state. Figure 4A shows a reference measurement at 4.2 K using the sequence shown in Fig. 2A, but with XY-16 decoupling. In Fig. 4B, the D^+ nuclear spins are placed into a coherent superposition at 4.2 K, the XY-16 sequence is begun, and then the temperature is ramped to room temperature in ~ 6 min. It is held there for 2 min before being ramped back down to 4.2 K in ~ 4 min. Once the sample is reimmersed in liquid He, the XY-16 sequence ends and the remaining coherence is projected back into a $\pm Z$ state for readout after reneutralization. By comparing the two readout signals we see that it is possible to bring a coherent state from cryogenic temperature to room temperature and back while retaining 62% of the coherence signal, which is equivalent to a state fidelity of 81% (22). This loss of coherence can be largely attributed to the $\sim 30\%$ drop in nuclear spin polarization observed over one thermal cycle to room temperature and back.

These results support the possibility of truly long-term storage of quantum information at room temperature. To make use of the D^+ state as a quantum memory for, say, a donor-based electron spin qubit, as has already been done with the nuclear spin of D^0 (23), it will be necessary to find a

way to ionize and neutralize the donor without disturbing the coherent state of the nuclear spin. Whereas ^{31}P donors in ^{28}Si at this time require low temperatures for initialization and readout, the ability to bring coherent information reversibly between cryogenic and room temperatures suggests ways to exploit this system. It may also be possible to initialize and read out this system at elevated temperatures, or to find similar but more robust systems with larger electron binding energies, in which charge control can still be used to turn a hyperfine interaction on for initialization and readout and off for long-term storage. In Si, one possibility would be to use much deeper donors such as chalcogens, where an optically accessible hyperfine splitting has already been observed for $^{77}\text{Se}^+$ in ^{28}Si (24) and where the hyperfine coupling can be removed by placing the donor into either D^0 or D^{2+} charge states. Another promising possibility would be deep defects in wider-gap materials such as diamond and SiC (25), which can also be isotopically purified to remove background spins and where the method of charge-state control could be combined with initialization and readout at room temperature.

References and Notes

1. D. Deutsch, *Proc. R. Soc. London Ser. A* **400**, 97–117 (1985).
2. T. D. Ladd *et al.*, *Nature* **464**, 45–53 (2010).
3. S. Wiesner, *ACM SIGACT News* **15**, 78–88 (1983).
4. F. Pastawski, N. Y. Yao, L. Jiang, M. D. Lukin, J. I. Cirac, *Proc. Natl. Acad. Sci. U.S.A.* **109**, 16079–16082 (2012).
5. P. C. Maurer *et al.*, *Science* **336**, 1283–1286 (2012).
6. B. E. Kane, *Nature* **393**, 133–137 (1998).
7. J. J. Morton, D. R. McCamey, M. A. Eriksson, S. A. Lyon, *Nature* **479**, 345–353 (2011).

8. D. D. Awschalom, L. C. Bassett, A. S. Dzurak, E. L. Hu, J. R. Petta, *Science* **339**, 1174–1179 (2013).
9. M. Steger *et al.*, *Science* **336**, 1280–1283 (2012).
10. G. Feher, E. A. Gere, *Phys. Rev.* **114**, 1245–1256 (1959).
11. L. Dreher, F. Hoehne, M. Stutzmann, M. S. Brandt, *Phys. Rev. Lett.* **108**, 027602 (2012).
12. J. J. Pla *et al.*, *Nature* **496**, 334–338 (2013).
13. W. M. Witzel, M. S. Carroll, Ł. Cywiński, S. Das Sarma, *Phys. Rev. B* **86**, 035452 (2012).
14. Supplementary materials are available on Science Online.
15. P. Dirksen, A. Henstra, W. Th. Wenckebach, *J. Phys. Condens. Matter* **1**, 7085–7092 (1989).
16. M. Steger *et al.*, *J. Appl. Phys.* **109**, 102411 (2011).
17. W. Schmid, *Phys. Status Solidi* **84**, 529–540 (1977) (b).
18. D. R. McCamey, J. Van Tol, G. W. Morley, C. Boehme, *Science* **330**, 1652–1656 (2010).
19. T. Gullion, D. B. Baker, M. S. Conradi, *J. Magn. Reson.* **89**, 479–484 (1990).
20. W. Burger, K. Lassmann, *Phys. Rev. Lett.* **53**, 2035–2037 (1984).
21. T. D. Ladd, D. Maryenko, Y. Yamamoto, E. Abe, K. M. Itoh, *Phys. Rev. B* **71**, 014401 (2005).
22. R. Jozsa, *J. Mod. Opt.* **41**, 2315–2323 (1994).
23. J. J. L. Morton *et al.*, *Nature* **455**, 1085–1088 (2008).
24. M. Steger *et al.*, *Phys. Rev. B* **80**, 115204 (2009).
25. W. F. Koehl, B. B. Buckley, F. J. Heremans, G. Calusine, D. D. Awschalom, *Nature* **479**, 84–87 (2011).

Acknowledgments: The work at Simon Fraser University was supported by the Natural Sciences and Engineering Research Council of Canada. S.S. is supported by the Violette and Samuel Glasstone Fellowship and St. John's College, Oxford. J.J.L.M. is supported by the Royal Society.

Supplementary Materials

www.sciencemag.org/content/342/6160/830/suppl/DC1
Materials and Methods
Supplementary Text
Figs. S1 to S3
References (26–37)

24 April 2013; accepted 15 October 2013
10.1126/science.1239584

Layer-Resolved Graphene Transfer via Engineered Strain Layers

Jeewan Kim,*† Hongsik Park,*† James B. Hannon, Stephen W. Bedell, Keith Fogel, Devendra K. Sadana, Christos Dimitrakopoulos*‡

The performance of optimized graphene devices is ultimately determined by the quality of the graphene itself. Graphene grown on copper foils is often wrinkled, and the orientation of the graphene cannot be controlled. Graphene grown on SiC(0001) via the decomposition of the surface has a single orientation, but its thickness cannot be easily limited to one layer. We describe a method in which a graphene film of one or two monolayers grown on SiC is exfoliated via the stress induced with a Ni film and transferred to another substrate. The excess graphene is selectively removed with a second exfoliation process with a Au film, resulting in a monolayer graphene film that is continuous and single-oriented.

Graphene offers great potential for high-performance electrical and optical devices such as radio-frequency transistors, high-speed photodetectors, and optical modulators (1–5). The most common approach used to build graphene devices is to grow the polycrystal-

line graphene via chemical vapor deposition on a thin metal foil, followed by transfer of the graphene to the substrate of interest (6, 7). This process can produce large areas of graphene with good control over the thickness. However, the graphene is often wrinkled because the metal foil substrate is rough. Furthermore, the relative crystallographic orientation of the domains is random because of the lack of registry with the substrate.

High-quality flat monolayer graphene can be epitaxially grown on the Si face of SiC (0001) wafers via a practically self-limiting sublimation of Si (8–10). Because of the high cost of SiC

IBM T. J. Watson Research Center, 1101 Kitchawan Road, Yorktown Heights, NY 10598, USA.

*Corresponding author. E-mail: jeewankim@us.ibm.com (J.K.); hpark@us.ibm.com (H.P.); dimitrak@umass.edu (C.D.)

†These authors contributed equally to this work.

‡Present address: University of Massachusetts, 686 North Pleasant Street, Amherst, MA 01003, USA.